



ELSEVIER

Contents lists available at ScienceDirect

Applied Mathematical Modelling

journal homepage: www.elsevier.com/locate/apm

A study on the method of fundamental solutions using an image concept

Jeng-Tzong Chen^{a,b,*}, Hung-Chih Shieh^a, Jhen-Jyun Tsai^a, Jia-Wei Lee^a

^a Department of Harbor and River Engineering, National Taiwan Ocean University, Keelung 20224, Taiwan

^b Department of Mechanical and Mechatronic Engineering, National Taiwan Ocean University, Keelung 20224, Taiwan

ARTICLE INFO

Article history:

Received 1 October 2009

Received in revised form 24 April 2010

Accepted 28 April 2010

Available online 9 May 2010

Keywords:

Method of fundamental solutions

Image method

Green's function

Boundary value problem

ABSTRACT

In this paper, both analytical and semi-analytical solutions for Green's functions are obtained by using the image method which can be seen as a special case of method of fundamental solutions (MFS). The image method is employed to solve the Green's function for the annular, eccentric and half-plane Laplace problems. In addition, an analytical solution is derived for the fixed-free annular case. For the half-plane problem with a circular hole and an eccentric annulus, semi-analytical solutions are both obtained by using the image concept after determining the strengths of two frozen image points and a free constant by matching boundary conditions. It is found that two frozen images terminated at the two foci in the bipolar coordinates for the problems with two circular boundaries. A boundary value problem of an eccentric annulus without sources is also considered. Error distribution is plotted after comparing with the analytical solution derived by Lebedev et al. using the bipolar coordinates. The optimal locations for the source distribution in the MFS are also examined by using the image concept. It is observed that we should locate singularities on the two foci to obtain better results in the MFS. Besides, whether the free constant is required or not in the MFS is also studied. The results are compared well with the analytical solutions.

© 2010 Elsevier Inc. All rights reserved.

1. Introduction

Method of fundamental solutions (MFS) has been developed for more than 50 years. The method was proposed by Kupradze and Aleksidze [1] in Russia since 1964. In the potential theory, it is well known that the MFS can solve potential problems if fundamental solutions of the partial differential equation are given. The Green's function has been studied and applied in many fields by mathematicians as well as engineers [2]. The fundamental solutions are free-space Green's functions while the Green's function is a fundamental solution with boundary conditions of a bounded domain. Both one contain a source in the domain. For the image method, Thomson [3] proposed the concept of reciprocal radii to find the image source to satisfy the homogeneous boundary condition. Chen and Wu [4] proposed an alternative way to determine the location of image by employing the degenerate kernel. The Green's function of Laplace equation was obtained by using the image method for a simple case in the Greenberg's book [5]. The Green's function of a circular ring has been solved using the complex variable by Courant and Hilbert [6]. In the Milne-Thomson book [7], he also used the technique of complex variables to solve the harmonic problems with circular boundaries. In the Chen and Wu [4] approach, we introduced the degenerate kernel to find the location of the image point. We admitted that various approaches may result in the same solution. However, we can extend the present approach to solve 3D problems but the method of complex variables may have difficulty. A successful

* Corresponding author at: Department of Harbor and River Engineering, National Taiwan Ocean University, Keelung 20224, Taiwan. Tel.: +886 2 24622192; fax: +886 2 24632375.

E-mail address: jtchen@mail.ntou.edu.tw (J.-T. Chen).

extension to 3D case can be found in the paper [8]. The optimal location of the MFS is also found by using the image method. We used the image method to obtain the Green's functions in the present paper. Mathematically speaking, we derive the Green's function by superimposing the fundamental solutions where singularities are located outside the domain. Therefore,

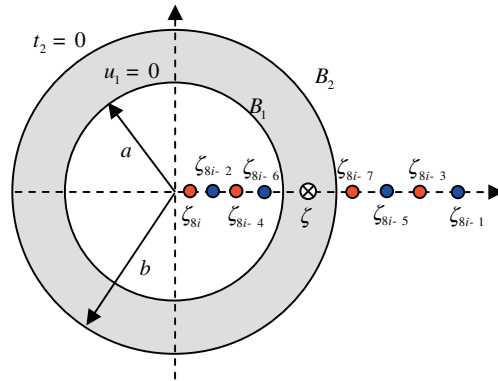
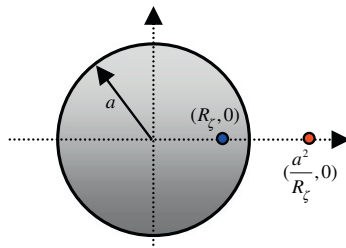
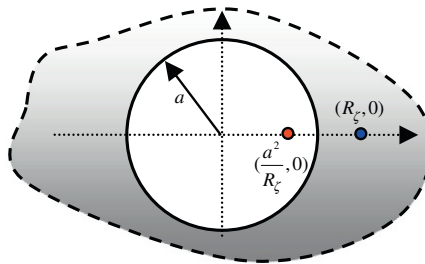


Fig. 1. Sketch of an annular problem.



(a) Interior problem



(b) Exterior problem

Fig. 2. Sketch of image location: (a) interior case and (b) exterior case.

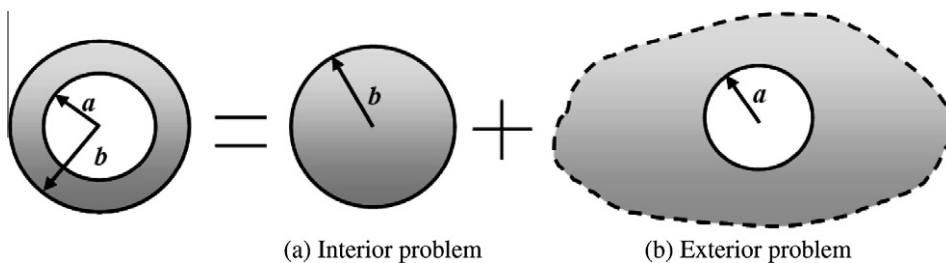


Fig. 3. An annular case composed of (a) interior and (b) exterior cases.

the image method can be seen as a special case of the MFS since all the image sources are located outside the domain. To derive the Green's function for problems with circular boundaries by using the image method is the main concern of this

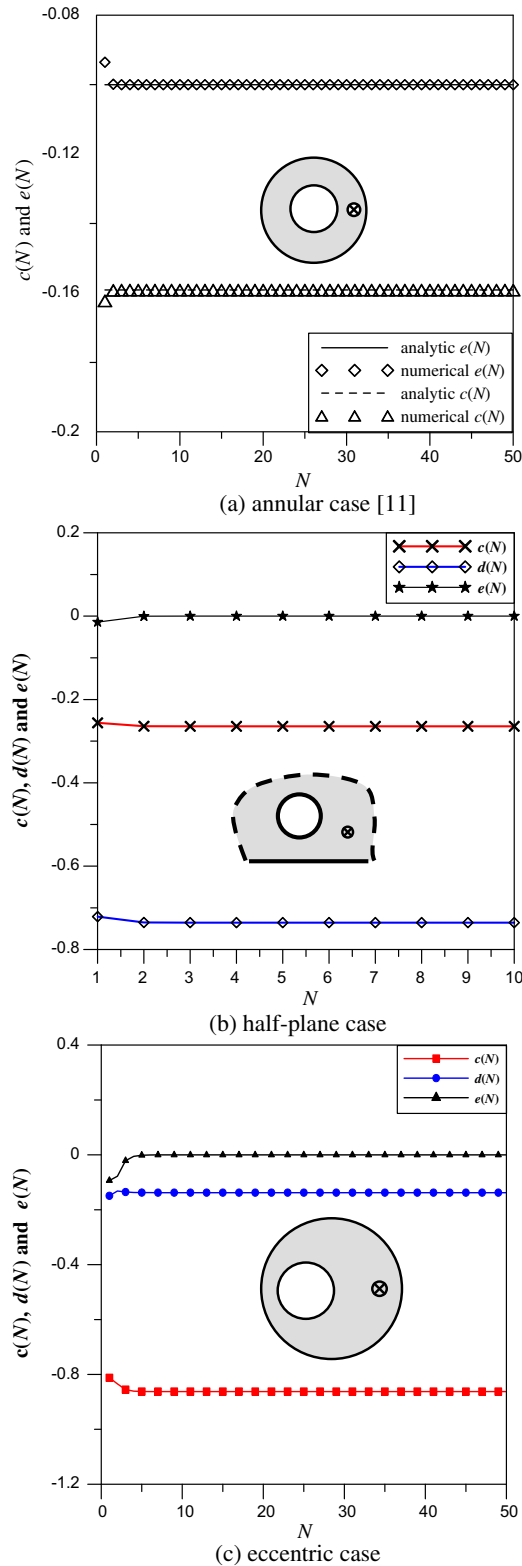


Fig. 4. Values of $c(N)$, $d(N)$ and $e(N)$: (a) annular case [11], (b) half-plane case and (c) eccentric case.

paper. Here, we put singularities along the radial direction in the method of images instead of angular distributions for the annular case.

In this paper, both analytical and semi-analytical solutions for the Green's functions of annular, eccentric and half-plane problems are derived. The analytical solutions for the fixed-free annulus are obtained by using the image method in conjunction with the addition theorem or the so-called degenerate kernel. For the semi-analytical solution, a half-plane problem with a circular hole and an eccentric annulus are considered to demonstrate that the image method can capture the optimal location of MFS sources. The agreement between the semi-analytical solution and that of null-field boundary integral equation method (BIEM) is examined. Following the successful experiences on the derivation of Green's function, we extend to solve the boundary value problem without sources by using the MFS. Saavedra and Power [9] have discussed the role of free constant in the MFS. As quoted by [9], "However, usually it is necessary to add a constant term in particular in two dimensions, where it is required for completeness purposes. As can be observed a constant value is always a solution of the Laplace's equation." Whether it is necessary for adding a constant in the MFS formulation is a nontrivial issue. It is interesting to find that only the strengths at the two foci for the eccentric annulus are required, if the rigid body term is considered in the MFS. When the conventional MFS without adding a constant term is used, how to represent the constant field by superimposing the singularities becomes an interesting issue. Error distribution is plotted after comparing with the analytical solutions of Lebedev et al. [10]. The optimal location in the MFS highly correlates to the two foci for the problem of eccentric annulus. Numerical results of eccentric case are compared with the analytical solution using the bipolar coordinates.

2. An analytical solution for the Green's function of annular region by using the image method

For a two-dimensional annular problem as shown in Fig. 1, the Green's function satisfies

$$\nabla^2 G(x, \zeta) = \delta(x - \zeta), \quad x \in \Omega, \tag{1}$$

where Ω is the domain of interest and δ denotes the Dirac-delta function for the source at ζ . For simplicity, the Green's function is considered to be subject to the fixed-free boundary conditions

$$G(x, \zeta) = 0, \quad x \in B_1, \tag{2}$$

$$\frac{\partial G(x, \zeta)}{\partial n_x} = 0, \quad x \in B_2, \tag{3}$$

where B_1 and B_2 are the inner and outer boundaries, respectively. As mentioned in the book of Courant and Hilbert [6], the interior and exterior Green's functions can satisfy the fixed-free boundary conditions if the image source is correctly selected. The closed-form Green's functions for both interior and exterior problems are written to be the same form

$$G(x, \zeta) = \ln |x - \zeta| - \ln |x - \zeta'| + \ln a - \ln R_\zeta, \quad x \in \Omega, \tag{4}$$

where a is the radius of the circle, $\zeta = (R_\zeta, 0)$, R_ζ is the distance from the source to the center of the circle, ζ' is the image source and its position is at $(a^2/R_\zeta, 0)$ as shown in Fig. 2. Fig. 1 depicts a series of images for the annular problems. We consider the fundamental solution $U(x, s)$ for a source singularity at s which satisfies

$$\nabla^2 U(x, s) = 2\pi\delta(x - s). \tag{5}$$

Then, we obtain the fundamental solution as follows:

$$U(x, s) = \ln r, \tag{6}$$

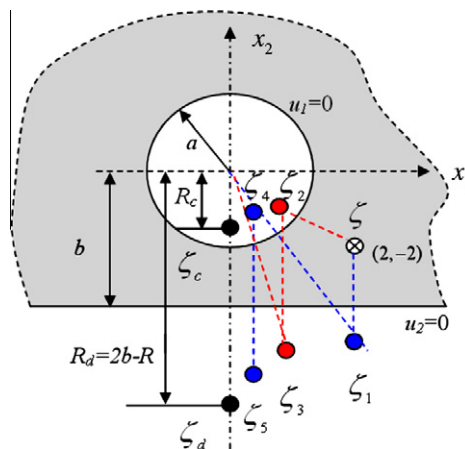


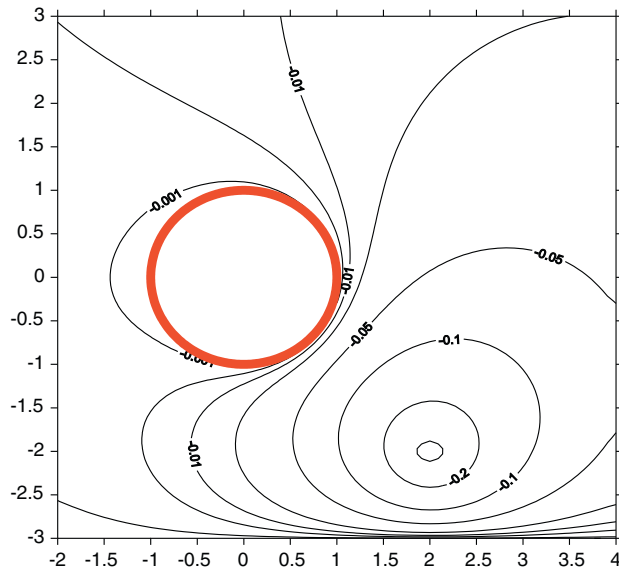
Fig. 5. A half-plane problem with a circular hole and its images.

where r is the distance between s and x ($r \equiv |x - s|$). Based on the separable property of addition theorem or degenerate kernel, the fundamental solution $U(x, s)$ is expanded into a series form by separating the field point $x(\rho, \varphi)$ and source point $s(R, \theta)$ in the polar coordinates [4]:

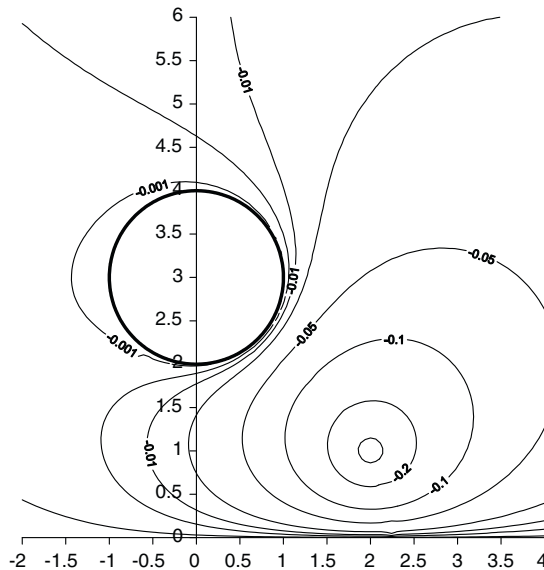
$$U(x, s) = \begin{cases} U^I(\rho, \phi; R, \theta) = \ln R - \sum_{m=1}^{\infty} \frac{1}{m} \left(\frac{\rho}{R}\right)^m \cos m(\theta - \phi), & R \geq \rho, \\ U^E(\rho, \phi; R, \theta) = \ln \rho - \sum_{m=1}^{\infty} \frac{1}{m} \left(\frac{R}{\rho}\right)^m \cos m(\theta - \phi), & R < \rho, \end{cases} \quad (7)$$

where the superscripts of I and E denote the interior and exterior regions, respectively.

Now let us extend a circular case to an annular case. An annular case can be seen as a combination of an interior and an exterior problems as shown in Fig. 3. By matching the fixed-free boundary conditions for the inner and outer boundaries, we introduce image points ζ_1 and ζ_2 , respectively. Since ζ_2 results in the nonhomogeneous boundary conditions on the outer boundary, we need to introduce an extra image point ζ_3 . Similarly, ζ_1 results in the nonhomogeneous boundary conditions



(a) image method



(b) null-field BIEM

Fig. 6. Contour plots by using (a) image method and (b) null-field BIEM.

on the inner boundary and an additional image point ζ_4 is also required. By repeating the same procedure, we have a series of image sources locating at

$$\zeta_{8i-7} = \frac{b^2}{R_c} \left(\frac{b^4}{a^4}\right)^{i-1}, \quad \zeta_{8i-5} = \frac{b^2 R_c}{a^2} \left(\frac{b^4}{a^4}\right)^{i-1}, \quad \zeta_{8i-3} = \frac{b^4}{a^2 R_c} \left(\frac{b^4}{a^4}\right)^{i-1}, \quad \zeta_{8i-1} = \frac{b^4 R_c}{a^4} \left(\frac{b^4}{a^4}\right)^{i-1}, \quad i \in N, \tag{8}$$

$$\zeta_{8i-6} = \left(\frac{a^2}{R_c}\right) \left(\frac{a^4}{b^4}\right)^{i-1}, \quad \zeta_{8i-4} = \frac{a^2 R_c}{b^2} \left(\frac{a^4}{b^4}\right)^{i-1}, \quad \zeta_{8i-2} = \left(\frac{a^4}{b^2 R_c}\right) \left(\frac{a^4}{b^4}\right)^{i-1}, \quad \zeta_{8i} = \frac{a^4 R_c}{b^4} \left(\frac{a^4}{b^4}\right)^{i-1}, \quad i \in N. \tag{9}$$

Following the successive image process, it is found that the final two image locations freeze at the origin and infinity. There are two strengths of singularities to be determined. Therefore, the total Green's function is rewritten as

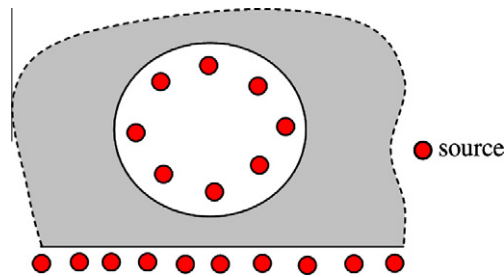


Fig. 7. Conventional MFS.

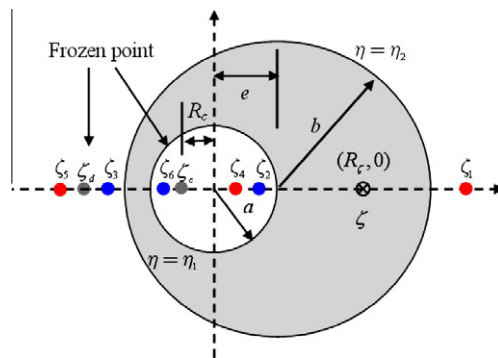


Fig. 8. Sketch of an eccentric problem subject to a concentrated load and the final two images at ζ_c and ζ_d .

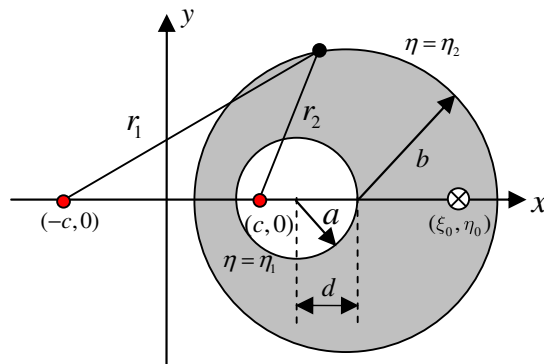
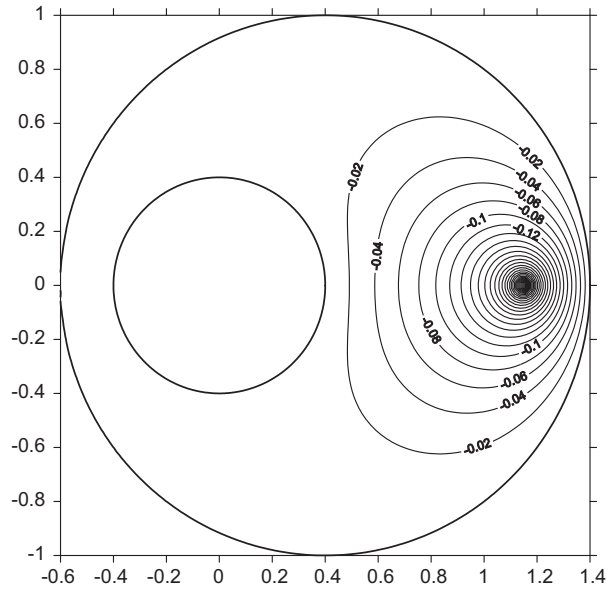


Fig. 9. Geometry relation of the bipolar coordinates.

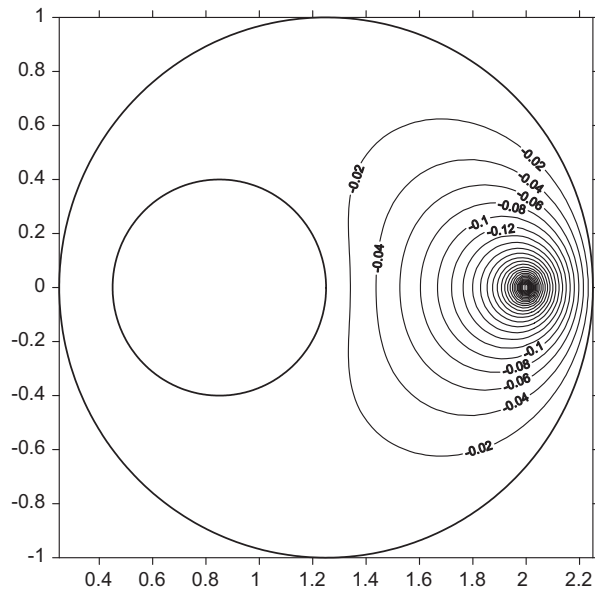
$$G(x, \zeta) = \frac{1}{2\pi} \left\{ \left[\ln|x - \zeta| + \lim_{N \rightarrow \infty} \left[\sum_{i=1}^N (\ln|x - \zeta_{8i-7}| - \ln|x - \zeta_{8i-6}| - \ln|x - \zeta_{8i-5}| - \ln|x - \zeta_{8i-4}|) \right. \right. \right. \\ \left. \left. \left. - \ln|x - \zeta_{8i-3}| + \ln|x - \zeta_{8i-2}| + \ln|x - \zeta_{8i-1}| + \ln|x - \zeta_{8i}| \right] + c(N) \ln \rho + e(N) \right] \right\}, \quad (10)$$

where $c(N)$ and $e(N)$ are the unknown coefficients which may be analytically and numerically determined by matching the inner and outer boundary conditions. To match the outer free boundary condition, the normal derivative of Eq. (10) yields

$$\frac{\partial G(x, \zeta)}{\partial n_x} = \frac{1}{2\pi} \frac{\partial}{\partial n_x} \left\{ \left[\ln|x - \zeta| + \lim_{N \rightarrow \infty} \left[\sum_{i=1}^N (\ln|x - \zeta_{8i-7}| - \ln|x - \zeta_{8i-6}| - \ln|x - \zeta_{8i-5}| - \ln|x - \zeta_{8i-4}|) \right. \right. \right. \\ \left. \left. \left. - \ln|x - \zeta_{8i-3}| + \ln|x - \zeta_{8i-2}| + \ln|x - \zeta_{8i-1}| + \ln|x - \zeta_{8i}| \right] + c(N) \ln \rho + e(N) \right] \right\} \quad (11)$$



(a) image method



(b) bipolar coordinates

Fig. 10. Contour plots for the eccentric solutions by using (a) image method and (b) analytical solution in terms of the bipolar coordinates.

In the real computation, we only used the finite N number of sources in the summation instead of double series of the eigenfunction expansion. The efficiency and convergence of solutions is observed for the unknown coefficients versus N as shown in Fig. 4. The Green's function of Eq. (10) is totally different from the double summation form in the textbook. By substituting the inner and outer boundary conditions into Eqs. (10) and (11) and using the addition theorem (degenerate kernel), the analytical forms of $c(N)$ and $e(N)$ are obtained as

$$\begin{Bmatrix} c(N) \\ e(N) \end{Bmatrix} = \begin{Bmatrix} -1 \\ \ln a - \ln R_c \end{Bmatrix}. \tag{12}$$

Numerically speaking, the values of unknown $c(N)$ and $e(N)$ can be alternatively determined by matching the inner and outer boundary conditions at two selected collocation points. The obtained numerical values of $c(N)$ and $e(N)$ agree well with the analytical result of Eq. (12) as shown in Fig. 4a. The generality of the present method over the complex variable approach for various boundary conditions can be found in [11].

3. Semi-analytical solutions for the half-plane problem with a circular hole and the eccentric ring by using the image method

Following the success of annular case for the iterative images, we now extend to the half-plane problem with a circular hole as shown in Fig. 5. In a similar way of finding the image for matching the inner boundary condition, an image is found. Besides, the reflection image point is needed to match the boundary condition on the ground surface. However, the two additional images, one inside the hole and the other under the ground line, result in new images to match the boundary condition of ground surface and inner circle, respectively. The iterative images and their locations are shown in Fig. 5. Two frozen images are found as the number of images becomes infinity. The locations of two frozen images are governed by

$$R_c = \frac{a^2}{R_d}, \quad R_d = 2b - R_c, \tag{13}$$

where a , b , R_c and R_d are shown in Fig. 5. Therefore, the Green's function is represented by

$$G(x, \zeta) = \frac{1}{2\pi} \left\{ \ln|x - \zeta| - \lim_{N \rightarrow \infty} \left[\sum_{i=1}^N (\ln|x - \zeta_{4i-3}| + \ln|x - \zeta_{4i-2}| - \ln|x - \zeta_{4i-1}| - \ln|x - \zeta_{4i}|) \right. \right. \\ \left. \left. + c(N) \ln|x - \zeta_c| + d(N) \ln|x - \zeta_d| + e(N) \right] \right\}, \tag{14}$$

where ζ_c and ζ_d are the location of the final two images, $c(N)$, $d(N)$ and $e(N)$ need to be determined by matching the boundary conditions. Based on the idea of MFS, we can say that not only some MFS sources are optimally located by using the image method but also the strengths except the two frozen images are also determined. Only three unknown coefficients are required to be determined by matching the boundary condition. This is quite different from the MFS since all the strengths need to be determined in a larger linear algebraic system. Numerical values for $c(N)$, $d(N)$, $e(N)$ versus N are shown in Fig. 4b. The contour plots by using the present method and the null-field BIEM [12] are shown in Fig. 6. It is found that good agreement is made after comparing our result with that of the null-field BIEM.

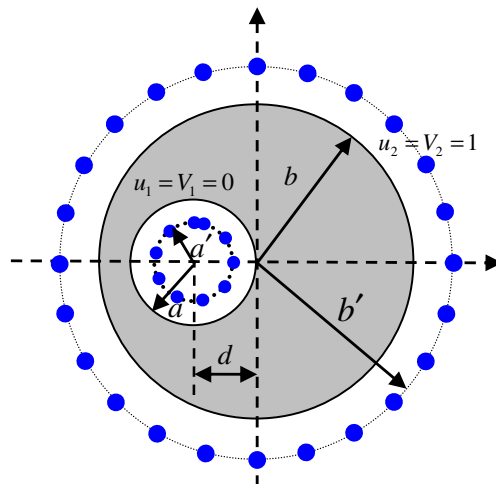


Fig. 11. Sketch of an eccentric annulus without sources.

Instead of using the conventional MFS as shown in Fig. 7, this image method can be seen as a special case of MFS with optimal locations of sources. Besides, the strengths of all the singularities are determined in advance except the singularity strengths of the two frozen images and one free constant. Similarly, we can extend the semi-analytical approach to solve the Green's function of eccentric case. The final locations of two image points are governed by

$$R_c = \frac{b^2}{R_d - e} + e, \quad R_d = \frac{a^2}{R_c}, \tag{15}$$

where a, b, e, R_c and R_d are shown in Fig. 8. The two analytical frozen images (ζ_c and ζ_d) are shown in Fig. 8 and the numerical experiment also supports this result.

Numerical values for $c(N), d(N), e(N)$ versus N are shown in Fig. 4c. The analytical solution of series form in the bipolar coordinates was derived by Heyda [13] as shown below:

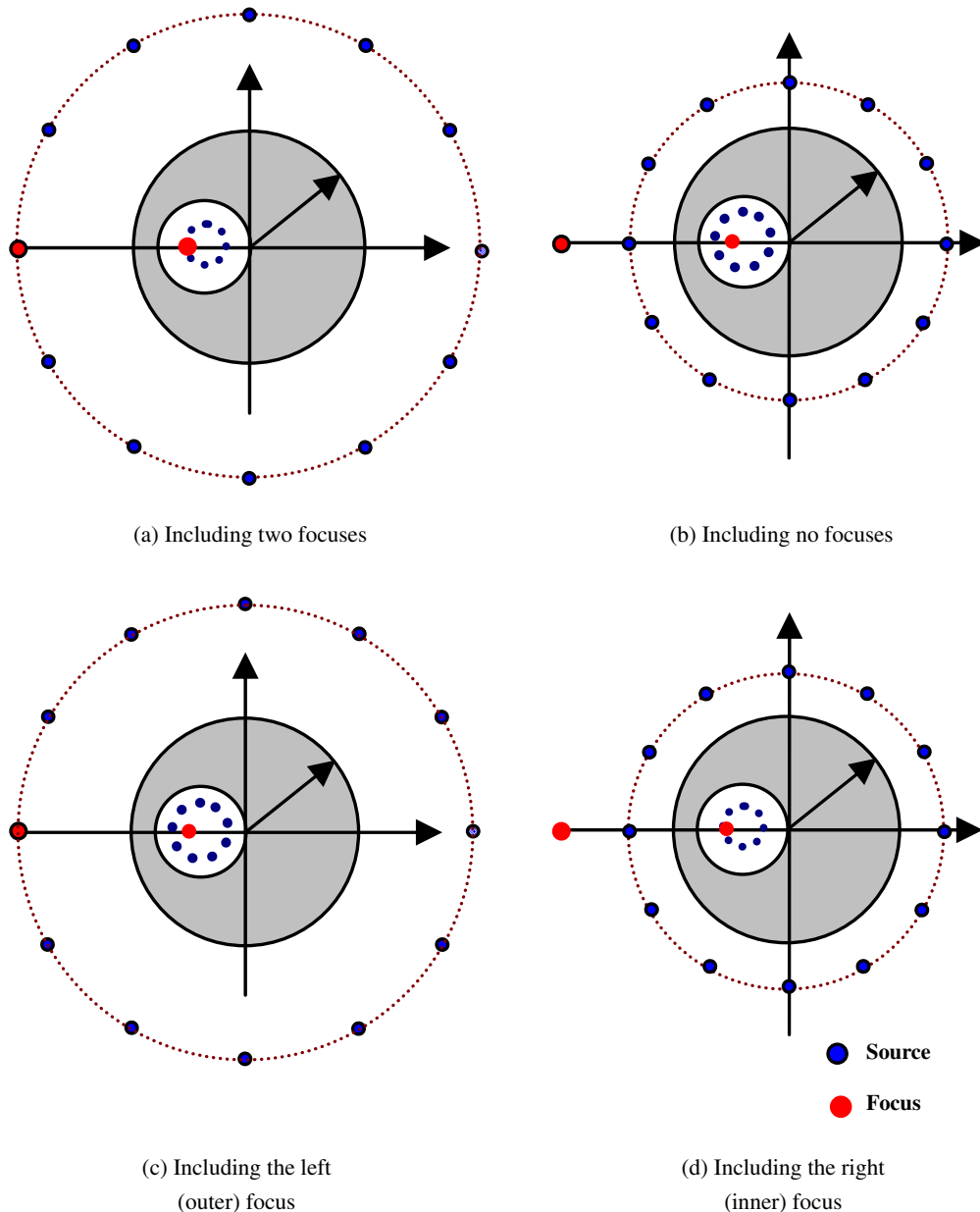


Fig. 12. Sketch of the source distribution in the MFS (a) including two focuses (b) including no focuses (c) including the left (outer) focus (d) including the right (inner) focus.

$$G(\xi, \eta; \xi_0, \eta_0) = \begin{cases} \frac{1}{2\pi} \left[\frac{(\eta_1 - \eta)(\eta_0 - \eta_2)}{\eta_1 - \eta_2} + 2 \sum_{n=1}^{\infty} \frac{\sinh n(\eta_1 - \eta) \sinh n(\eta_0 - \eta_2)}{n \sinh n(\eta_1 - \eta_2)} \cos n(\xi - \xi_0) \right], & \eta_1 < \eta < \eta_0, \\ \frac{1}{2\pi} \left[\frac{(\eta - \eta_2)(\eta_1 - \eta_0)}{\eta_1 - \eta_2} + 2 \sum_{n=1}^{\infty} \frac{\sinh n(\eta_1 - \eta_0) \sinh n(\eta - \eta_2)}{n \sinh n(\eta_1 - \eta_2)} \cos n(\xi - \xi_0) \right], & \eta_0 < \eta < \eta_2, \end{cases} \quad (16)$$

where (ξ, η) is the bipolar coordinates, $\eta = \eta_1$ and $\eta = \eta_2$ denote the inner and outer circles, respectively and (ξ_0, η_0) is the position of source point as shown in Fig. 9. The contour plots by using the present method and the analytical solution are shown in Fig. 10. Good agreement is observed.

4. Numerical solutions for an eccentric annulus without sources by using the MFS

In the foregoing section, we have derived the Green’s function of an eccentric case. In this section, we solve a boundary value problem without sources by using the MFS as shown in Fig. 11. The solution of MFS is written as

$$u(x) = \sum_{j=1}^N d_j U(x, s_j), \quad (17)$$

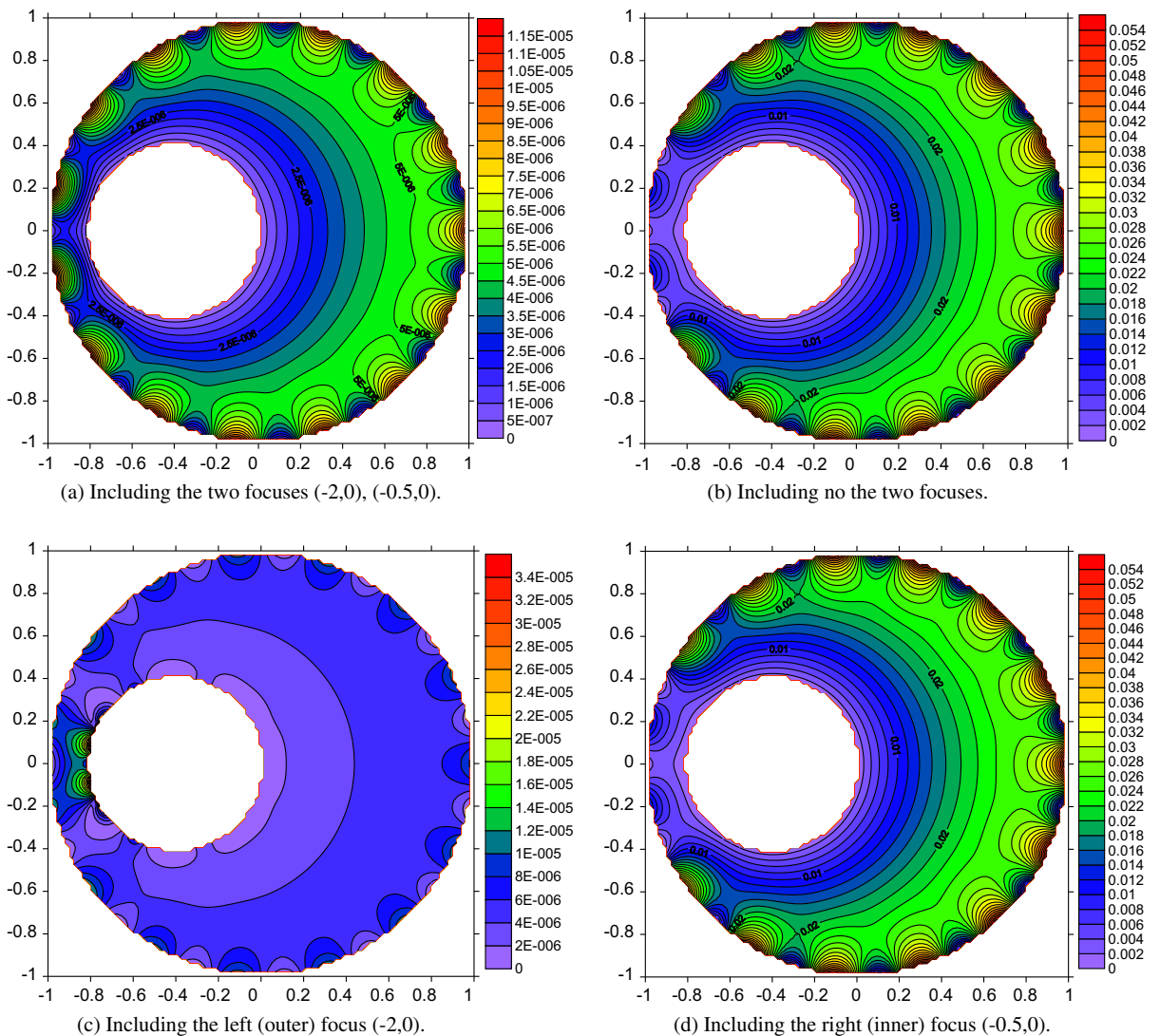


Fig. 13. Error distribution of source locations: (a) including the two foci $(-2, 0), (-0.5, 0)$, (b) including no the two foci, (c) including the left (outer) focus $(-2, 0)$ and (d) including the right (inner) focus $(-0.5, 0)$.

where N is the number of source points, d_j is the j th unknown coefficient. By matching the Dirichlet boundary conditions for the inner and outer boundaries, we can determine the unknown coefficients of d_j .

In the above cases for deriving the Green's function, we find that there are two frozen points by using the image method which locate on the two focuses in the bipolar coordinates. We suppose that the two frozen locations may also be very important for problems without sources. Here, we solve a boundary value problem of eccentric annulus by using the MFS. The pattern of source distribution is shown in Fig. 12 for (a) including two focuses, (b) including no focuses, (c) including the left (outer) focus and (d) including the right (inner) focus, respectively. The solutions of the MFS are compared with the analytical solution derived by Lebedev et al. [10]. The analytical solution of eccentric case obtained by using the bipolar coordinates is given below:

$$u(\xi, \eta) = A\eta + B = A(\ln r_1 - \ln r_2) + B, \tag{18}$$

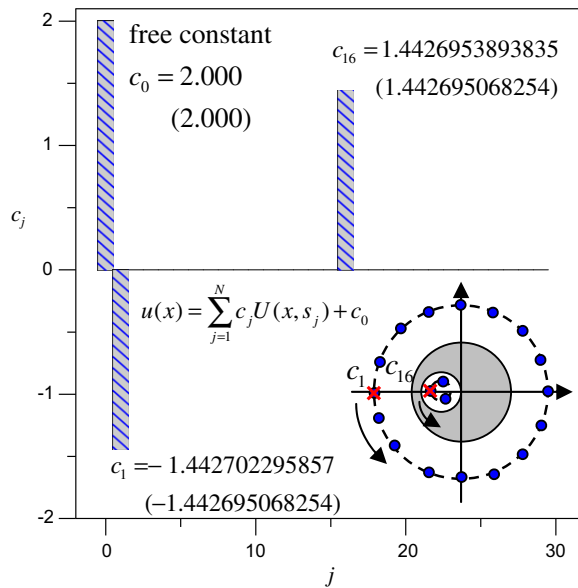


Fig. 14. Coefficient of c_j versus j by using Eq. (23) with a free constant, data in () denotes the analytical solution.

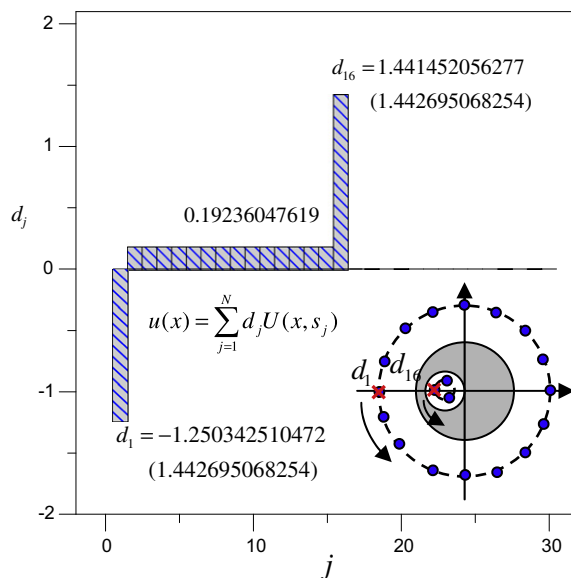


Fig. 15. Coefficient of d_j versus j by using Eq. (17) without a free constant.

where

$$A = \frac{V_1 - V_2}{\sinh^{-1}(\frac{c}{a}) - \sinh^{-1}(\frac{c}{b})} \tag{19}$$

$$B = V_1 - \frac{V_1 - V_2}{\sinh^{-1}(\frac{c}{a}) - \sinh^{-1}(\frac{c}{b})} \sinh^{-1}(\frac{c}{a}) \tag{20}$$

in which

$$c = \frac{\sqrt{a^4 - 2a^2b^2 + b^4 - 2a^2d^2 - 2b^2d^2 + d^4}}{2d} \tag{21}$$

Error distribution is defined by

$$\varepsilon(x) = \|u^N(x) - u^{exact}(x)\|, \quad x \in D, \tag{22}$$

and is shown in Fig. 13 for the source distribution (a) including the two focuses (−2, 0), (−0.5, 0), (b) not including the two focuses, (c) including one focus only (−2, 0) and (d) including one focus only (−0.5, 0), respectively. When the locations of sources include two focuses in Fig. 13a, we find that the numerical result best matches the analytical solution.

In the analytical solution of Eq. (18), there exists a rigid body term, *B*. For the MFS, Saavedra and Power [9] have pointed out that a free constant is needed for 2D problems in the MFS. Therefore, Eq. (17) is modified to

$$u(x) = \sum_{j=1}^N c_j U(x, s_j) + c_0, \tag{23}$$

where *c*₀ is a free constant and *c*_{*j*} is the unknown coefficient. When the source points are located along the two boundaries including two focuses as shown in Fig. 12a, we find that only the two nonzero strengths (*c*₁ and *c*₁₆) of singularities at the two focuses and the strength (*c*₀) happen to be equal to the coefficient of analytical solutions of Eqs. (19) and (20) and other weightings are all zeros, as shown in Fig. 14. The strengths of the two nonzero singularities are opposite to each other (*c*₁ = −*c*₁₆) as predicted by Eq. (18). This result can be analytically predicted. It indicates that we can approach the exact solution if a free constant is carefully added in the solution of MFS in advance. Unfortunately, the conventional MFS always employed Eq. (17) instead of Eq. (23). The key difference is a free constant. Fig. 15 shows that all singularities strengths in the

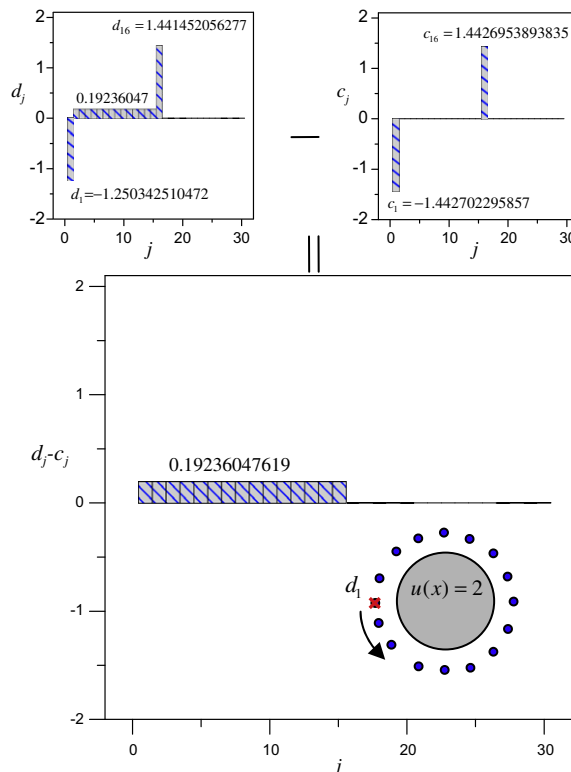


Fig. 16. Coefficient of *d*_{*j*} − *c*_{*j*} versus *j* to represent the constant field, *u*(*x*) = 2.

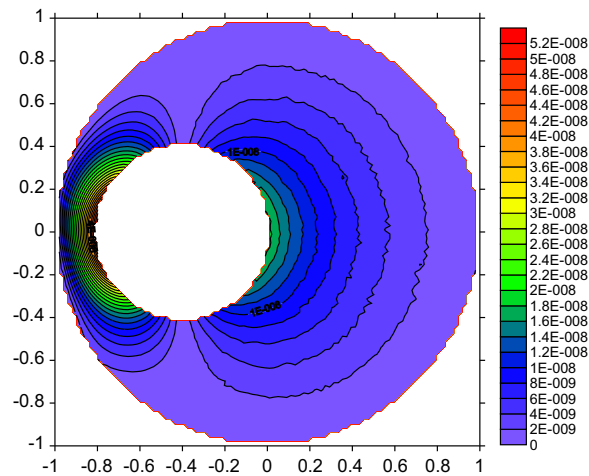


Fig. 17. Error distribution of source locations including the two foci $(-2, 0)$, $(-0.5, 0)$ by using Eq. (23).

inner sources are zeros except the one on the inner focus. If we use Eq. (17) free of a constant term, it is interesting to find the strengths ($d_1 \sim d_{15}$) of outer singularities are all nonzero and only one nonzero singularity (d_{16}) on the interior focus for inner singularities. It is interesting to find that the difference ($d_j - c_j$) of Fig. 14 (c_j) and Fig. 15 (d_j) can represent a constant interior field of $c_0 = 2$ as shown in Fig. 16. This result indicates that a constant interior field (c_0) can be superimposed by using outer instead of inner singularities when the MFS solution of Eq. (17) does not contain the constant term of interior field. In Fig. 17, error distribution of Eq. (22) using the MFS of Eq. (23) shows more accurate result than that using Eq. (17), because Eq. (23) approaches the analytical solution better than Eq. (17) does. Although Eq. (17) does not contain a free term, its solution is also acceptable since superposition of outer singularities can represent a constant field. It is noted that the free constant in the MFS is absolutely required for the exterior field containing a constant since this constant cannot be superimposed by using inner singularities.

5. Conclusions

In this paper, the analytical and semi-analytical solutions for the Green's functions of annulus and half-plane problems were obtained by using the image method. The numerical solutions for boundary value problems of an eccentric annulus were obtained by using the MFS. For the analytical solution of annular case, the image method (a special MFS) was employed to derive the analytical Green's function of fixed-free annulus. For the half-plane problem with a circular cavity, a semi-analytical solution was obtained by determining only one free constant and two strengths of singularities at the two frozen images. Agreement is observed after comparing with the result of null-field BIEM. Besides, the same idea of semi-analytical approach was successfully extended to solve the Green's function for the eccentric annulus. The semi-analytical results also agree well with the analytical solution by using the bipolar coordinates. The numerical solution of an eccentric annulus without the source was compared with analytical solutions. The MFS with or without adding a constant were employed to solve the eccentric annulus without a source. It is found that only two nonzero singularities at the foci and one constant are required to represent the analytical solution of eccentric annulus if the MFS containing an adding constant is used. This case can be seen as the simplest MFS that has only two source points and a constant. Even though the MFS without adding a constant is employed to solve the BVP of an eccentric annulus, acceptable results can be also obtained. The reason can be explained that a constant term can be superimposed by using uniform distribution of outer singularities. In the demonstrated example, the addition of free constant is not absolutely necessary according to the numerical experiments. However, the MFS including the free constant yields the best solution in the test example. The free constant in the MFS may play an important role for the solution of unbounded domain problem containing a rigid body term.

Acknowledgements

Financial support from the National Science Council under Grant No. NSC-98-2221-E-019-017-MY3 and NTOU-RD-AA-2010-104021 is gratefully acknowledged.

References

- [1] V.D. Kupradze, M.A. Aleksidze, A method for the approximate solution of limiting problems in mathematical physics, *Comput. Math. Math. Phys.* 4 (1964) 199–205.
- [2] M.A. Jaswon, G.T. Symm, *Integral Equation Methods in Potential Theory and Electrostatics*, Academic Press, New York, 1977.

- [3] W. Thomson, Maxwell in his treatise, quotes a paper in the Cambridge and Dublin Math., vol. I., 1848 (chapter XI).
- [4] J.T. Chen, C.S. Wu, Alternative derivations for the Poisson integral formula, *Int. J. Math. Educ. Sci. Technol.* 37 (2006) 165–185.
- [5] M.D. Greenberg, *Application of Green's Functions in Science and Engineering*, Prentice-Hill, New Jersey, 1971.
- [6] R. Courant, D. Hilbert, *Methods of Mathematical Physics*, Interscience, New York, 1953.
- [7] L.M. Milne-Thomson, *Theoretical Hydrodynamics*, Dover, New York, 1968.
- [8] J.T. Chen, H.C. Shieh, Y.T. Lee, J.W. Lee, Image solutions for boundary value problems without sources, *Appl. Math. Comput.* 216 (2010) 1453–1468.
- [9] I. Saavedra, H. Power, Multipole fast algorithm for the least-squares approach of the method of fundamental solutions for three-dimensional harmonic problems, *Numer. Methods Partial Differ. Eqn.* 19 (2003) 825–845.
- [10] N.N. Lebedev, I.P. Skalskaya, Y.S. Uflyand, *Worked Problems in Applied Mathematics*, Dover Publications, New York, 1979.
- [11] J.T. Chen, Y.T. Lee, S.R. Yu, S.C. Shieh, Equivalence between the Trefftz method and the method of fundamental solution for the annular Green's function using the addition theorem and image concept, *Eng. Anal. Bound. Elem.* 33 (2009) 678–688.
- [12] J.T. Chen, K.H. Chou, S.K. Kao, Derivation of Green's function using addition theorem, *Mech. Res. Commun.* 36 (2009) 351–363.
- [13] J.F. Heyda, A Green's function solution for the case of laminar incompressible flow between non-concentric circular cylinders, *J. Franklin Inst.* 267 (1959) 25–34.